Nonaffinity of Liquid Networks and Bicontinuous Mesophases

Michael S. Dimitriyev,[1,2,*] Xueyan Feng,[3] Edwin L. Thomas,[2] and Gregory M. Grason[1,†]
[1]Department of Polymer Science and Engineering, University of Massachusetts, Amherst, Massachusetts 01003, USA
[2]Department of Materials Science and Engineering, Texas A&M University, College Station, Texas 77843, USA
[3]Department of Macromolecular Science, State Key Laboratory of Molecular Engineering of Polymers, Fudan University, Shanghai, China 200438

(Received 13 November 2023; revised 21 January 2024; accepted 28 March 2024; published 23 May 2024)

Amphiphiles self-assemble into a variety of bicontinuous mesophases whose equilibrium structures take the form of high-symmetry cubic networks. Here, we show that the symmetry-breaking distortions in these systems give rise to anomalously large, nonaffine collective deformations, which we argue to be a generic consequence of "mass equilibration" within deformed networks. We propose and study a minimal "liquid network" model of bicontinuous networks, in which acubic distortions are modeled by the relaxation of residually stressed mechanical networks with constant-tension bonds. We show that nonaffinity is strongly dependent on the valency of the network as well as the degree of strain-softening or strain-stiffening tension in the bonds. Taking diblock copolymer melts as a model system, liquid network theory captures quantitative features of two bicontinuous phases based on comparison with self-consistent field theory predictions and direct experimental characterization of acubic distortions, which are likely to be pronounced in soft amphiphilic systems more generally.

DOI: 10.1103/PhysRevLett.132.218201

The self-assembly of amphiphiles into mesophases with long-range order is of fundamental importance to the formation of structure in biology and nanotechnology. Beyond the classical lamellar, columnar, and sphere mesophases, there are a variety of bicontinuous mesophases, from amorphous sponges to triply periodic double networks. Of the latter, the double gyroid (DG), double diamond (DD), and double primitive (DP), closely related to triply periodic (cubic) minimal surfaces, are most commonly observed [1–3]. The combination of highly symmetric morphologies and complex topologies of these structures underlie valuable functional properties, from structural coloration in living organisms [4–6] to photonic [7,8] and plasmonic metamaterials [9,10].

In contrast to atomic or molecular crystals, supramolecular crystals, such as the bicontinuous networks, contain upward of $\sim 10^4$ macromolecules per unit cell, allowing for more complex distortions. As shown in Fig. 1(a), bicontinuous networks are typically visualized as interconnected tubular domains, separated by slablike matrices or membranes [11]. It is useful to decompose these structures into mesoatomic units that represent collective groupings centered on the nodal interconnections: DG, DD, and DP mesoatoms are, respectively, three, four, and six valent [12,13]. Further abstraction of the network domains yields a "skeletal graph" representation [see Fig. 1(c)] with nodes centered within the mesoatoms and "struts" joining each node. Recent observations of DG [14] and DD [15] crystals assembled by block copolymers—subject to endemic sources of symmetry-breaking stresses (e.g., due to anisotropic solvent processing and inadequate thermal relaxation via sample annealing)—exhibit strong, coherent distortions of the otherwise cubic unit cells [Fig. 1(b)].

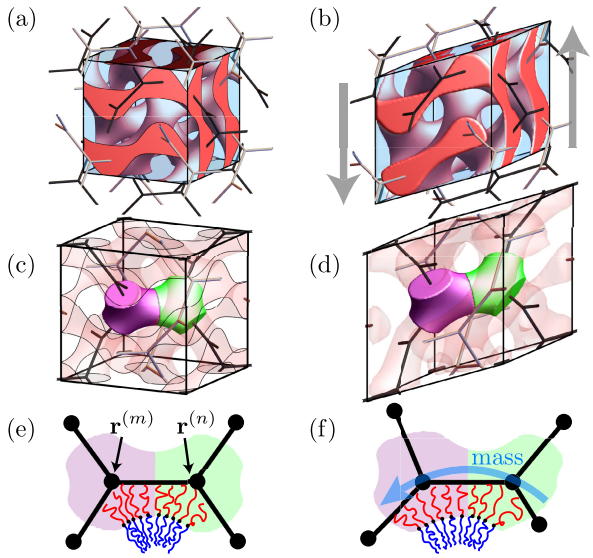

FIG. 1. Unit cells of a DG composed of tubular domains (red) separated by a continuous matrix domain (blue) and disjoint skeletal networks from SCF calculations, (a) with full cubic symmetry and (b) after a simple shear. (c),(d) Neighboring "mesoatomic units" highlighted in magenta and green, before and after the simple shear, respectively. Schematic arrangement of diblock copolymers with mesoatom pairs, at nodal positions $\mathbf{r}^{(m)}$ and $\mathbf{r}^{(n)}$, possessing equal chain numbers for cubic structures (e) and net transfer of mass upon symmetry-breaking shear (f).

Experimental reconstructions show a combination of anomalously large fluctuations in strut lengths, yet surprisingly low deviations in bond angles. This observation hints at the exotic mechanics underlying network relaxation, characterized by pronounced *nonaffine* response. While rigid, amorphous soft materials, such as biopolymer networks, proteins, foams, and gels, have well-characterized nonaffinity [16–27], and nonaffine fluctuations have been studied in crystalline solids [28–30], the mechanism behind the nonaffine response in supramolecular networks—structured fluids with crystalline order—is apparently fundamentally distinct. Notably, nonaffine and symmetry-breaking distortions are thought to be important for the self-assembly of Weyl metamaterials [31–33].

In this Letter, we explore the relaxation of supramolecular networks in response to broken cubic symmetry, through the lens of liquid network theory (LNT) as a proxy for collective intranetwork mass redistribution [Fig. 1(b)]. Constant-tension networks exhibit highly nonaffine response, which is a strong function of nodal valence and symmetry with a linear response encoded in two cubic invariants coupled to simple and elongational shear. LNT predicts trihedral [34] DG (the 10-3a net [35]) to be generically more nonaffine than tetrahedral DD (the 6-4 net), a result that we directly confirm using a combination of self-consistent field (SCF) theory and experimental tomographic reconstructions of acubic network phases of block copolymers. More generally, we connect this regime of pronounced nonaffine relaxation in perfectly ordered networks to the presence of strain-softening central forces between nodes.

Skeletal network degrees of freedom are specified by node positions $\{\mathbf{r}^{(n)}\}$, along with strut-sharing, nearest-neighbor node pairs $\langle mn\rangle$. We restrict our attention to network deformations that maintain the number of nodes and the connectivity of the graph. We take these node positions as the effective, coarse-grained degrees of freedom and consider the simplest form of the free energy H that can account for internodal mass exchange, composed of nearest-neighbor interactions of the form $H = \sum_{\langle mn\rangle} h(\ell^{(mn)})$, where $\ell^{(mn)} \equiv |\mathbf{r}^{(n)} - \mathbf{r}^{(m)}|$ is the length of the strut joining node m to node n and h is an energy per strut. The equilibrium condition then requires a balance of forces at each node, i.e., $\sum_{n\in\langle mn\rangle} \tau(\ell^{(mn)})\hat{\mathbf{r}}^{(mn)} = 0$, where $\hat{\mathbf{r}}^{(mn)}$ is the unit vector joining node n to node m, and $\tau(\ell) \equiv \mathrm{d}h/\mathrm{d}\ell$ is the corresponding tension along the strut.

Generic equilibrium conditions for macromolecular assemblies involve a balance of enthalpic costs due to maintaining an interface between unlike components (referred to as the intermaterial dividing surface for amphiphilic morphologies) and entropic costs associated with molecular configurations (e.g., reductions in entropy due to stretching polymers) [36,37]. As depicted in Fig. 1(e), macromolecules typically orient normal to the struts; restoring forces due to changes in molecular conformation are thus transverse to the strut. However, macromolecules can easily translate along a network and even hop between distinct networks (albeit with a free energy barrier); as shown in Fig. 1(f), deformations can result in easy intranetwork transfer of mass between mesoatoms. Associating each macromolecule to the nearest strut and assuming the areal density of molecules passing through the interface to be approximately constant, the mass per strut is roughly proportional to the strut length ℓ. Consequently, to maintain chemical equilibrium in the network, τ is length independent [$\tau(\ell) = \text{const}$]; this is the constitutive relationship for LNT. Notably, length-minimizing triply periodic networks with fixed valency are known to correspond to the cubic skeletons of DG, DD, and DP [38,39].

To explore the behavior of LNT, we first consider the planar three-strut graph shown in Fig. 2(a), whose initial configuration of struts with equal length ℓ_0 and angle of 120° results in mechanical equilibrium for the central node for any constitutive form of $\tau(\ell)$. The boundary nodes are then affinely displaced by stretching along the direction $\hat{\mathbf{d}}$ by a factor ε; the deformation matrix is $\Lambda_{ij} = \delta_{ij} + \varepsilon\hat{d}_i\hat{d}_j$. Finally, relaxation of the central node, while holding boundary nodes fixed, results in a displacement $\mathbf{u}$, as depicted in Fig. 2(b); a nonzero value of $\mathbf{u}$ indicates a nonaffine deformation of the graph. For LNT (constant tension), equilibrium requires strut angles maintain 120° coordination, which generally necessitates a nonaffine displacement of the central node. This can be regarded as a 1D version of Plateau's laws for soap films [40,41]. Beyond trihedral graphs, equilibrium conditions for LNT require strut orientations to sum to zero at each node. Thus, nodes exhibiting tetrahedral and hexahedral symmetry, such as those seen in DD and DP, are LNT equilibria, as are the more exotic pentahedral nodes seen in DD mirror twin boundaries [15]. More generally, we can consider a broader class of power-law constitutive relations

$$\tau(\ell) = \tau_0\left(\frac{\ell}{\ell_0}\right)^{\eta}, \tag{1}$$

where τ_0 is the residual tension of struts in the initial configuration. The exponent η controls the character of the mechanical response, as shown in Fig. 2(c): for $\eta = 1$, the struts obey Hooke's law; for $0 < \eta < 1$, the network strain softens; for $\eta > 1$, the network strain stiffens; $\eta = 0$ corresponds to LNT (i.e. constant tension). The increasing magnitude of nonaffine deformation $|\mathbf{u}|^2$ with strain ε varies with η, as shown in Fig. 2(c). This measure of the nonaffine response increases quadratically with strain, $|\mathbf{u}|^2/\ell_0^2 = \Gamma\varepsilon^2$, as is generally expected for mechanical networks for $\varepsilon \ll 1$, where Γ is the "nonaffinity" parameter [19,21,22,42,43]. We find that LNT is characterized by especially large values of Γ, compared to strain-stiffening

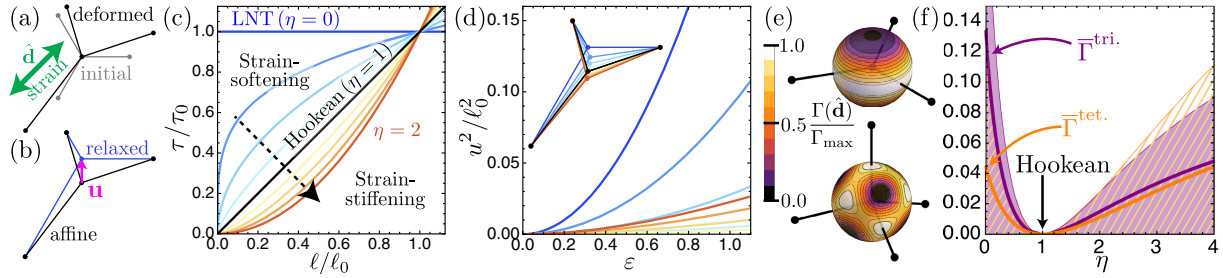

FIG. 2. (a) Three-strut planar graph with initial strut lengths ℓ_0 and angle of 120° between neighboring struts, superposed with affinely stretched variant (along $\hat{\mathbf{d}}$, in the plane). (b) Nonaffine relaxation, characterized by central node displacement $\mathbf{u}$ under equilibrium of LNT. (c) Power-law constitutive relations for tension $\tau(\ell)$ as a function of length ℓ. (d) Nonaffine displacement $|\mathbf{u}|^2/\ell_0^2$, as a function of strain ε. (e) Spherical map of direction-dependent nonaffinity $\Gamma \equiv |\mathbf{u}|^2/(\ell_0^2\varepsilon^2)$ for a trihedral (top) and a tetrahedral (bottom) graph. (f) Average nonaffine response for trihedral and tetrahedral graphs as a function of η. Shaded regions represent the full range of $\Gamma(\hat{\mathbf{d}})$.

forces that are typical of many fiber networks [24,44–47]. As shown in Supplemental Material [48], similar values can be achieved in finitely extensible flexible and semiflexible polymer networks [55,56], but only in the highly non-Hookean, high-extension limit. Moreover, the volume constraint ensures that struts maintain nonzero tension and places LNT in a similar class of residually stressed mechanical networks as those described by the classical description of rubber elasticity [57,58], involving Hookean networks with affine response, independent of network geometry [59]. This residual stress stabilizes the sub-isostatic DG and DD networks, despite their low valency (with valence $z < 6$) [60,61], which in turn alters expectations for the dependence of nonaffinity on total valence. The effect of pre-stress to stabilize otherwise floppy networks has recently been recognized in the context athermal fiber networks [62], and more classically, underlies the success of classical theories of rubber/gel elasticity [59].

Next, consider trihedral and tetrahedral graphs in 3D, representing a nodal region in DG and DD, respectively. The resulting nonaffinity parameter $\Gamma(\hat{\mathbf{d}})$ has a directional dependence that is plotted on the unit sphere, superimposed on both graphs in Fig. 2(e); by symmetry of the uniaxial deformation, $\Gamma(-\hat{\mathbf{d}}) = \Gamma(\hat{\mathbf{d}})$. The restoring force from each strut is proportional to the projection of the strut direction onto the stretch direction $\hat{\mathbf{d}}$; consequently, the DP hexahedral nodes always maintain affine deformations. The nonaffine response is therefore maximal along the strut directions for both graphs and is zero along the threefold axis (out-of-plane normal) of the trihedral graph and along each of the fourfold rotoinversion axes of the tetrahedral graph. The full range of the nonaffinity parameter for both graphs is shown in Fig. 2(f). We see that LNT has the largest nonaffine response for both networks over a broad range of non-negative values of η, with larger values for the tetrahedral graph when $\eta > 4$; as $\eta \to \infty$, the maximal values of Γ^{tri} and Γ^{tet} approach $1/4$ and $4/9$, respectively. Moreover, the trihedral graph exhibits a consistently larger maximum of the nonaffinity parameter for small η; the tetrahedral graph becomes more nonaffine than the trihedral for $\eta > 2$. Since networks may contain trihedral or tetrahedral nodes (or both for (3,4) nets [35] and certain Fischer-Koch structures [63]) with a variety of orientations, it is useful to quantify the averaged response for both types of nodes, which we obtain by averaging $\Gamma(\hat{\mathbf{d}})$ over all possible stretching directions on the unit sphere. The resulting averaged nonaffinity $\bar{\Gamma}$ is plotted in Fig. 2(f); note that $\bar{\Gamma}^{\text{tri}}/\bar{\Gamma}^{\text{tet}} = 3$ (see Supplemental Material [48]).

Next, we turn to the linear response of full DG and DD networks at fixed volume; calculation details are shown in Supplemental Material [48]. Given a general deformation matrix $\mathbf{\Lambda}$, the nonaffine response is a function of the strain tensor, $\boldsymbol{\varepsilon} = (\mathbf{\Lambda}^T\mathbf{\Lambda} - \mathbb{1})/2$, which is, by construction, symmetric and invariant under rigid rotations of the network [64]. The nonaffine response can be characterized by $\langle|\mathbf{u}|^2\rangle$, where the average is taken over all nodes in a unit cell. In the linear response regime, the quadratic scaling with ε_{ij} is characterized by a nonaffinity tensor Γ^{ijkl} and takes on the form

$$\frac{\langle|\mathbf{u}|^2\rangle}{\ell_0^2} = \Gamma^{ijkl}\varepsilon_{ij}\varepsilon_{kl} = \Gamma_{\text{ext}}\sum_i \frac{\hat{\varepsilon}_{ii}^2}{2} + \Gamma_{\text{shear}}\sum_{i\neq j}\hat{\varepsilon}_{ij}^2, \quad (2)$$

where $\hat{\varepsilon}_{ij} \equiv \varepsilon_{ij} - \varepsilon_{kk}\delta_{ij}/3$ is the deviatoric (i.e., traceless) strain. For the cubic networks considered here, we can express the tensor in terms of two independent components, Γ_{ext} and Γ_{shear}, representing the response to volume-preserving extensional and shear strains, respectively (see Supplemental Material [48]).

The resulting extensional and shear components of the nonaffinity tensor are given in Table I for general values of η. LNT predicts a ratio between the nonaffine response to shear deformation $\Gamma_{\text{shear}}^{\text{DG}}/\Gamma_{\text{shear}}^{\text{DD}} = 3$ that is in agreement with average nonaffinity ratio of the trihedral and tetrahedral nodes. For DD, because the extensional strain involves compression and elongation along the [100] family of directions relative to the unit cell, which align with the

TABLE I. Components of the cubic nonaffinity tensor Γ for DG and DD, for generic (Gen. η) power-law strut tension $\tau(\ell) \propto \ell^{\eta}$, LNT, and SCF theory linear diblock copolymer melts.

	$\Gamma^{\mathrm{DG}}_{\mathrm{ext}}$	$\Gamma^{\mathrm{DG}}_{\mathrm{shear}}$	$\Gamma^{\mathrm{DD}}_{\mathrm{ext}}$	$\Gamma^{\mathrm{DD}}_{\mathrm{shear}}$
Gen. η	$\frac{3}{4}[(1-\eta)/(1+3\eta)]^2$	$\frac{1}{8}[(1-\eta)/(1+\eta)]^2$	0	$\frac{1}{6}[(1-\eta)/(2+\eta)]^2$
LNT	0.75	0.125	0	$\approx$0.042
SCF	$0.20_{\pm 0.02}$	$0.17_{\pm 0.02}$	$0.02_{\pm 0.01}$	$0.28_{\pm 0.02}$

rotoinversion axes of the tetrahedral nodes, $\Gamma^{\mathrm{DD}}_{\mathrm{ext}}$ is uniformly zero for all values of η. Notably, for general $\eta > 0$, $\Gamma^{\mathrm{DG}}_{\mathrm{ext}}$ becomes smaller than $\Gamma^{\mathrm{DG}}_{\mathrm{shear}}$. While our results suggest an apparent decrease in non-affinity with valence, we emphasize that certain features of the response are consequences of particular symmetries of networks. For example, generic affinity of DP is a consequence of (local) nodal symmetry, in which affine deformation preserve collinearity of force-balancing struts in all three independent directions. For DD, the perfectly affine response for extensions along [100] directions relies on global registry of nodal response (i.e. black directions in Fig. 2(e)) along crystallographic directions. Hence, in an "amorphous" network of tetrahedral nodes (e.g. in a disordered bicontinuous sponge), we expect non-affinity along extension in all directions, as well as the possibility of additional instabilities due to structural inhomogeneities in a disordered network [65].

Now we consider our results in the context of diblock copolymers (BCPs), based on experiments involving DG and DD networks formed from polystyrene-*b*-polydimethylsiloxane (PS-PDMS), as well as associated SCF calculations of equilibrium structures (see Supplemental Material [48]). First, we performed a series of SCF computations that explore the equilibrium morphologies formed by BCPs when the cubic symmetry of the DG-DD unit cell is broken by an applied affine transformation $\mathbf{\Lambda}$. Using a skeletonization algorithm, we determined the nonaffine displacements $\langle|\mathbf{u}|^2\rangle$ of nodes along separate extensional and shear strain deformation paths (see Supplemental Material [48]). This way, we were able to measure nonaffinity components from SCF calculations, shown in Table I. For DG, we found that the shear component is comparable to predictions of LNT, but the extensional component is somewhat smaller than expected. This significant depression of $\Gamma^{\mathrm{DG}}_{\mathrm{ext}}$ suggests that terms beyond LNT may prove important for certain strain directions; indeed, our mechanical network model suggests that a small, nonzero value of η is needed to capture this scale of nonaffinity. While such a fractional tension-length constitutive relationship is unlikely to have a clear physical interpretation, our use of η in the power-law form $\tau(\ell)$ given in Eq. (1) is simply to facilitate the analysis in this Letter. As shown in Supplemental Material [48], our results hold under a much more general set of constitutive relationships $\tau(\ell)$, wherein $\eta = \ell\tau'/\tau$, which will generically depend on deformation. SCF calculations show a small, nonzero value for $\Gamma^{\mathrm{DD}}_{\mathrm{ext}}$ as well as a larger-than-expected value of $\Gamma^{\mathrm{DD}}_{\mathrm{shear}}$. Such discrepancies suggest that effects beyond the minimal LNT, such as internetwork interactions, may play a larger role in the response of DD.

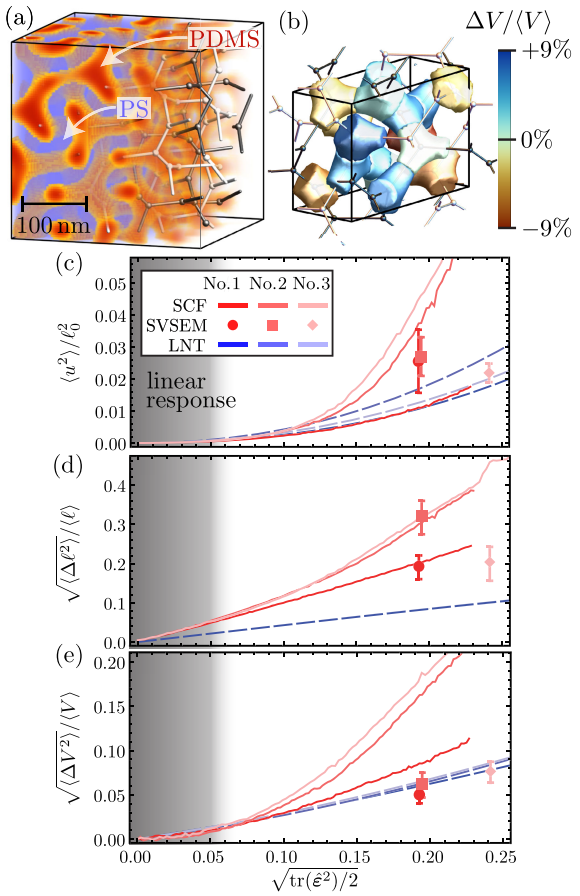

FIG. 3. (a) 3D tomographic reconstruction from SVSEM data of a DG grain from PS-PDMS thin film, with extracted skeletal graph. (b) Distribution of nodal volumes in a 3D construction of a unit cell in DG sample No. 1, showing $\sim \pm 9\%$ variations in volume. Below, plots show (c) average nonaffine displacement $\langle|\mathbf{u}|^2\rangle$, (d) strut length variations $\sqrt{\langle\Delta\ell^2\rangle}/\langle\ell\rangle$, and (e) variance in nodal volume $\sqrt{\langle\Delta V^2\rangle}/\langle V\rangle$, for experiments (markers), simulated deformation paths from SCF calculations (red curves), and corresponding LNT predictions (blue, dashed curves) as a function of total strain $\sqrt{\mathrm{tr}(\hat{\boldsymbol{\varepsilon}}^2)/2}$.

We analyzed prior experimental data, which consist of 3D density fields extracted using "slice-and-view" scanning electron microscopy (SVSEM) [12,14]. This technique yields nanometer-scale voxels representing local density measurements of PDMS relative to PS, resulting in 3D reconstructions, such as shown in Fig. 3(a), which then can be skeletonized using a similar algorithm as used for the density fields obtained from SCF calculations [66]. The experimental data include structures sampled from three distinct grains of a DG polycrystal and two distinct grains of a DD polycrystal. While each of the grains possess distinct triclinically deformed unit cells (obtained from Fourier analysis of the density field data), we can compare against predictions of LNT and molecular SCF theory by simulating constant-volume deformations paths that include the triclinic unit cells for each of the grains (i.e., maintaining roughly constant ratios of shear to extensional strain). The average nonaffine displacement along each family of deformations for the DG samples is shown in Fig. 3(b) for SCF calculations and LNT, along with experimental measurements; note that the error bars come from unit-cell averaged measurement of nonaffine displacement from multiple unit cells within each 3D reconstruction. We plot these distinct deformation paths, which combine mixtures of extensional and shear strain, as functions of a common strain measure $\sqrt{\mathrm{tr}(\hat{\boldsymbol{\epsilon}}^2)/2}$, a combination of extensional and shear strain (see Supplemental Material [48]). While there is good agreement between LNT and SCF for low strain, SCF results depart from LNT predictions for strain values on the order of 5%–10%. For larger strains, the nonaffine response attains significant nonquadratic contributions involving higher order couplings between extensional and shear strain that fall well outside of the linear response regime. Nevertheless, we note that the parameter-free LNT does a remarkable job in capturing the magnitude of nonaffinity for the experimental DG samples, which evidently exhibit significant acubic distortion (≈20%). Further studies involving careful processing and annealing are needed to fully relax the networks and may result in better agreement between experiment and theory.

Finally, we address our central hypothesis that mass transport plays a key role in the equilibration of deformed networks. Since we assumed that macromolecules associate with struts, the variance in strut length, shown in Fig. 3(c), is related to fluctuations in the total mass of molecules associated with a given strut. These fluctuations may originate from variations in macromolecule density and conformations at constant mass per strut and thus involve elastic contributions to the strut tension. A different measure of mass transport is the variation in the volume per node (or mesoatom), determined by counting the mass contribution per voxel and associating each voxel to the nearest node in space (see Supplemental Material [48]). For example, a single unit cell from an experimental sample shows ∼10% variation in volume between nodes [see Fig. 3(b)] that are equivalent in the undeformed, cubic configuration. Applying the same method to the DG grains and simulated deformation paths, we find that variance in nodal volume increases with strain and again, as shown in Fig. 3(e), LNT exhibits a smaller variance than SCF calculations as well as experimental measurements.

We have shown that, to a first approximation, the collective response of supramolecular networks to symmetry-breaking deformations is controlled by equilibration of mass along network elements, captured via a simple principle of length minimization. While both experiment and SCF theory exhibit near-quantitative and fit-free agreement with LNT in the linear response regime, it is clear that additional contributions from macromolecule elasticity as well as packing constraints (and thus intranetwork interactions) are needed, particularly in the large-strain regime. Nevertheless, LNT naturally explains prior observations of "rigid" strut angle relationships and "soft" strut length requirements for BCP network deformations and defects [14,15]. Furthermore, LNT can rationalize an observed "node-splitting" transition observed in DD (see Supplemental Material [48]), particularly under modest extensional strain, where tetrahedral nodes split into pairs of trihedral nodes. Since LNT equilibria correspond to locally length-minimizing networks, node-splitting events tend toward globally length-minimizing configurations, known as "Steiner networks," composed of purely trihedral nodes [38,39]. As such, LNT provides a minimal basis for understanding deformations of supramolecular networks well beyond linear response, into the regime of defects and structural transitions.

The authors thank B. Greenvall for stimulating discussions and valuable comments on this work. This research was supported by the U.S. Department of Energy (DOE), Office of Basic Energy Sciences, Division of Materials Sciences and Engineering, under Award No. DE-SC0022229. SCF computations were performed on the Unity Cluster at the Massachusetts Green High Performance Computing Center.

*msdim@tamu.edu
†grason@umass.edu

[1] L. E. Scriven, Equilibrium bicontinuous structure, Nature (London) **263**, 123 (1976).
[2] E. L. Thomas, D. M. Anderson, C. S. Henkee, and D. Hoffman, Periodic area-minimizing surfaces in block copolymers, Nature (London) **334**, 598 (1988).
[3] J. N. Israelachvili, 20—soft and biological structures, in *Intermolecular and Surface Forces (Third Edition)*, edited by J. N. Israelachvili (Academic Press, San Diego, 2011), pp. 535–576.
[4] J. W. Galusha, L. R. Richey, J. S. Gardner, J. N. Cha, and M. H. Bartl, Discovery of a diamond-based photonic crystal

structure in beetle scales, Phys. Rev. E **77**, 050904(R) (2008).
[5] V. Saranathan, C. O. Osuji, S. G. J. Mochrie, H. Noh, S. Narayanan, A. Sandy, E. R. Dufresne, and R. O. Prum, Structure, function, and self-assembly of single network gyroid (I4132) photonic crystals in butterfly wing scales, Proc. Natl. Acad. Sci. U.S.A. **107**, 11676 (2010).
[6] V. Saranathan, S. Narayanan, A. Sandy, E. R. Dufresne, and R. O. Prum, Evolution of single gyroid photonic crystals in bird feathers, Proc. Natl. Acad. Sci. U.S.A. **118**, e2101357118 (2021).
[7] K. Hur, Y. Francescato, V. Giannini, S. A. Maier, R. G. Hennig, and U. Wiesner, Three-dimensionally isotropic negative refractive index materials from block copolymer self-assembled chiral gyroid networks, Angew. Chem., Int. Ed. **50**, 11985 (2011).
[8] J.-H. Lee, C. Y. Koh, J. P. Singer, S.-J. Jeon, M. Maldovan, O. Stein, and E. L. Thomas, 25th anniversary article: Ordered polymer structures for the engineering of photons and phonons, Adv. Mater. **26**, 532 (2014).
[9] P. A. Mistark, S. Park, S. E. Yalcin, D. H. Lee, O. Yavuzcetin, M. T. Tuominen, T. P. Russell, and M. Achermann, Block-copolymer-based plasmonic nanostructures, ACS Nano **3**, 3987 (2009).
[10] S. Vignolini, N. A. Yufa, P. S. Cunha, S. Guldin, I. Rushkin, M. Stefik, K. Hur, U. Wiesner, J. J. Baumberg, and U. Steiner, A 3d optical metamaterial made by self-assembly, Adv. Mater. **24**, OP23 (2012).
[11] S. Hyde, B. W. Ninham, S. Andersson, K. Larsson, T. Landh, Z. Blum, and S. Lidin, Beyond flatland: The geometric forms due to self-assembly, in *The Language of Shape*, edited by S. Hyde, B. W. Ninham, S. Andersson, K. Larsson, T. Landh, Z. Blum, and S. Lidin (Elsevier Science B.V., Amsterdam, 1997), Chap. 4, pp. 141–197.
[12] A. Reddy, X. Feng, E. L. Thomas, and G. M. Grason, Block copolymers beneath the surface: Measuring and modeling complex morphology at the subdomain scale, Macromolecules **54**, 9223 (2021).
[13] G. M. Grason and E. L. Thomas, How does your gyroid grow? A mesoatomic perspective on supramolecular, soft matter network crystals, Phys. Rev. Mater. **7**, 045603 (2023).
[14] X. Feng, C. J. Burke, M. Zhou, H. Guo, K. Yang, A. Reddy, I. Prasad, R.-M. Ho, A. Avgeropoulos, G. M. Grason, and E. L. Thomas, Seeing mesoatomic distortions in soft-matter crystals of a double-gyroid block copolymer, Nature (London) **575**, 175 (2019).
[15] X. Feng, M. S. Dimitriyev, and E. L. Thomas, Soft, malleable double diamond twin, Proc. Natl. Acad. Sci. U.S.A. **120**, e2213441120 (2023).
[16] D. J. Durian, Foam mechanics at the bubble scale, Phys. Rev. Lett. **75**, 4780 (1995).
[17] S. A. Langer and A. J. Liu, Effect of random packing on stress relaxation in foam, J. Phys. Chem. B **101**, 8667 (1997).
[18] D. A. Head, A. J. Levine, and F. C. MacKintosh, Deformation of cross-linked semiflexible polymer networks, Phys. Rev. Lett. **91**, 108102 (2003).
[19] B. A. DiDonna and T. C. Lubensky, Nonaffine correlations in random elastic media, Phys. Rev. E **72**, 066619 (2005).
[20] E. Conti and F. C. MacKintosh, Cross-linked networks of stiff filaments exhibit negative normal stress, Phys. Rev. Lett. **102**, 088102 (2009).
[21] C. P. Broedersz, X. Mao, T. C. Lubensky, and F. C. MacKintosh, Criticality and isostaticity in fibre networks, Nat. Phys. **7**, 983 (2011).
[22] A. Basu, Q. Wen, X. Mao, T. C. Lubensky, P. A. Janmey, and A. G. Yodh, Nonaffine displacements in flexible polymer networks, Macromolecules **44**, 1671 (2011).
[23] E. M. Huisman and T. C. Lubensky, Internal stresses, normal modes, and nonaffinity in three-dimensional biopolymer networks, Phys. Rev. Lett. **106**, 088301 (2011).
[24] C. P. Broedersz and F. C. MacKintosh, Modeling semiflexible polymer networks, Rev. Mod. Phys. **86**, 995 (2014).
[25] J. Feng, H. Levine, X. Mao, and L. M. Sander, Nonlinear elasticity of disordered fiber networks, Soft Matter **12**, 1419 (2016).
[26] D. D. Prakashchand, N. Ahalawat, S. Bandyopadhyay, S. Sengupta, and J. Mondal, Nonaffine displacements encode collective conformational fluctuations in proteins, J. Chem. Theory Comput. **16**, 2508 (2020).
[27] M. Pensalfini, T. Golde, X. Trepat, and M. Arroyo, Nonaffine mechanics of entangled networks inspired by intermediate filaments, Phys. Rev. Lett. **131**, 058101 (2023).
[28] M. V. Jarić and U. Mohanty, Density-functional theory of elastic moduli: Hard-sphere and Lennard-Jones crystals, Phys. Rev. B **37**, 4441 (1988).
[29] S. Ganguly, S. Sengupta, P. Sollich, and M. Rao, Nonaffine displacements in crystalline solids in the harmonic limit, Phys. Rev. E **87**, 042801 (2013).
[30] T. Das, S. Ganguly, S. Sengupta, and M. Rao, Pre-yield nonaffine fluctuations and a hidden critical point in strained crystals, Sci. Rep. **5**, 10644 (2015).
[31] M. Fruchart, S.-Y. Jeon, K. Hur, V. Cheianov, U. Wiesner, and V. Vitelli, Soft self-assembly of Weyl materials for light and sound, Proc. Natl. Acad. Sci. U.S.A. **115**, E3655 (2018).
[32] S. Jo, H. Park, T. Jun, K. Kim, H. Jung, S. Park, B. Lee, S. Lee, and D. Y. Ryu, Symmetry-breaking in double gyroid block copolymer films by non-affine distortion, Appl. Mater. Today **23**, 101006 (2021).
[33] H. Park, S. Jo, B. Kang, K. Hur, S. S. Oh, D. Y. Ryu, and S. Lee, Block copolymer gyroids for nanophotonics: Significance of lattice transformations, Nanophotonics **11**, 2583 (2022).
[34] We opt to describe nodes as polyhedra, where each strut emerging from the node is represented by a face. DG nodes are described as trihedral; DD nodes are tetrahedral; DP nodes are hexahedral (described by octahedral symmetry group O_h).
[35] A. F. Wells, *Three Dimensional Nets and Polyhedra* (Wiley, New York, 1977).
[36] D. M. Anderson, S. M. Gruner, and S. Leibler, Geometrical aspects of the frustration in the cubic phases of lyotropic liquid crystals, Proc. Natl. Acad. Sci. U.S.A. **85**, 5364 (1988).
[37] M. W. Matsen and F. S. Bates, Origins of complex self-assembly in block copolymers, Macromolecules **29**, 7641 (1996).

[38] J. Alex and K. Grosse-Brauckmann, Periodic networks of fixed degree minimizing length, arXiv:1911.01792.
[39] J. Alex and K. Grosse-Brauckmann, Periodic Steiner networks minimizing length, Discrete Comput. Geom. **70**, 1145 (2023).
[40] C. Isenberg, *The Science of Soap Films and Soap Bubbles*, Dover Books Explaining Science (Dover Publications, New York, 1992).
[41] A. Ivanov and A. A. Tuzhilin, *Minimal Networks: The Steiner Problem and Its Generalizations* (CRC Press, Boca Raton, Florida, 1994).
[42] M. Wyart, H. Liang, A. Kabla, and L. Mahadevan, Elasticity of floppy and stiff random networks, Phys. Rev. Lett. **101**, 215501 (2008).
[43] J.-M. Y. Carrillo, F. C. MacKintosh, and A. V. Dobrynin, Nonlinear elasticity: From single chain to networks and gels, Macromolecules **46**, 3679 (2013).
[44] M. L. Gardel, J. H. Shin, F. C. MacKintosh, L. Mahadevan, P. Matsudaira, and D. A. Weitz, Elastic behavior of cross-linked and bundled actin networks, Science **304**, 1301 (2004).
[45] C. Storm, J. J. Pastore, F. C. MacKintosh, T. C. Lubensky, and P. A. Janmey, Nonlinear elasticity in biological gels, Nature (London) **435**, 191 (2005).
[46] O. Lieleg, M. M. A. E. Claessens, C. Heussinger, E. Frey, and A. R. Bausch, Mechanics of bundled semiflexible polymer networks, Phys. Rev. Lett. **99**, 088102 (2007).
[47] A. Sharma, A. J. Licup, K. A. Jansen, R. Rens, M. Sheinman, G. H. Koenderink, and F. C. MacKintosh, Strain-controlled criticality governs the nonlinear mechanics of fibre networks, Nat. Phys. **12**, 584 (2016).
[48] See Supplemental Material at http://link.aps.org/supplemental/10.1103/PhysRevLett.132.218201, for additional information about the simulation and experimental methods, as well as supplemental discussion, which includes Refs. [49–54].
[49] A. Arora, J. Qin, D. C. Morse, K. T. Delaney, G. H. Fredrickson, F. S. Bates, and K. D. Dorfman, Broadly accessible self-consistent field theory for block polymer materials discovery, Macromolecules **49**, 4675 (2016).
[50] M. Warner and E. Terentjev, *Liquid Crystal Elastomers*, International Series of Monographs on Physics (Oxford University Press, Oxford, 2007).
[51] A. Reddy, M. S. Dimitriyev, and G. M. Grason, Medial packing and elastic asymmetry stabilize the double-gyroid in block copolymers, Nat. Commun. **13**, 2629 (2022).
[52] M. S. Dimitriyev, A. Reddy, and G. M. Grason, Medial packing, frustration, and competing network phases in strongly segregated block copolymers, Macromolecules **56**, 7184 (2023).
[53] T. S. Bailey, C. M. Hardy, T. H. Epps, and F. S. Bates, A noncubic triply periodic network morphology in poly(isoprene-*b*-styrene-*b*-ethylene oxide) triblock copolymers, Macromolecules **35**, 7007 (2002).
[54] C. A. Tyler and D. C. Morse, Orthorhombic Fddd network in triblock and diblock copolymer melts, Phys. Rev. Lett. **94**, 208302 (2005).
[55] J. F. Marko and E. D. Siggia, Stretching DNA, Macromolecules **28**, 8759 (1995).
[56] M. Rubinstein and R. Colby, *Polymer Physics* (Oxford University Press, New York, 2003).
[57] L. Treloar, *The Physics of Rubber Elasticity*, Oxford Classic Texts in the Physical Sciences (Oxford University Press, Oxford, 1975).
[58] P. J. Flory, Molecular theory of rubber elasticity, Polym. J. **17**, 1 (1985).
[59] S. Alexander, Amorphous solids: Their structure, lattice dynamics and elasticity, Phys. Rep. **296**, 65 (1998).
[60] J. Clerk Maxwell, On the calculation of the equilibrium and stiffness of frames, London Edinburgh Philos. Mag. & J. Sci. **27**, 294 (1864).
[61] C.R. Calladine, Buckminster Fuller's "Tensegrity" structures and Clerk Maxwell's rules for the construction of stiff frames, Int. J. Solids Struct. **14**, 161 (1978).
[62] J. L. Shivers, S. Arzash, A. Sharma, and F. C. MacKintosh, Scaling theory for mechanical critical behavior in fiber networks, Phys. Rev. Lett. **122**, 188003 (2019).
[63] W. Fischer and E. Koch, Spanning minimal surfaces, Phil. Trans. R. Soc. A **354**, 2105 (1996).
[64] L. D. Landau, E. M. Lifshitz, A. M. Kosevich, and L. P. Pitaevskii, *Theory of Elasticity*, Course of Theoretical Physics (Butterworth-Heinemann, London, 1986).
[65] M. Baggioli, I. Kriuchevskyi, T. W. Sirk, and A. Zaccone, Plasticity in amorphous solids is mediated by topological defects in the displacement field, Phys. Rev. Lett. **127**, 015501 (2021).
[66] I. Prasad, H. Jinnai, R.-M. Ho, E. L. Thomas, and G. M. Grason, Anatomy of triply-periodic network assemblies: Characterizing skeletal and inter-domain surface geometry of block copolymer gyroids, Soft Matter **14**, 3612 (2018).